Journal of Alloys and Compounds 747 (2018) 1073–1077

Contents lists available at ScienceDirect

Journal of Alloys and Compounds

journal homepage: http://www.elsevier.com/locate/jalcom

Letter

Densification kinetics of flash sintered 3mol% Y_2O_3 stabilized zirconia

Keywords:
Flash sintering
Densification kinetics
Oxygen vacancies
Electrostatic interaction

A B S T R A C T

Flash sintering is an attractive technique that is capable of rapidly sintering ceramics, although its densification mechanism is arguable. Hence, studies involving the kinetics of flash sintering are crucial in providing insights into the ultrafast densification process. In this work, a 3mol% Y_2O_3 stabilized zirconia (3YSZ) was used as a model compound for determining flash sintering densification kinetics. Shrinkage of 3YSZ samples during the flash sintering process at 900 °C was recorded as a function of applied current density. Activation energy for the flash densification process was determined based on the conventional densification theory. Results indicated that the injected oxygen vacancies at the incubation stage had a direct influence on the densification activation energy. In contrast, the densification during the flash sintering stage appeared to be dominated by the migration of oxygen vacancies under an electric field. This was inferred upon by the comparison of activation energies for the densification and conduction processes. Based on this finding, we propose that flash densification results from the movement of oxygen vacancies to form different charged defects that have an electrostatic interaction between them.

1. Introduction

Flash sintering is a field assisted sintering technique (FAST) wherein a ceramic green-body is sintered to near full density for a few seconds at a certain temperature under an applied electric field. This process is accompanied by a non-linear increase in conductivity and power dissipation [1]. Since it was first reported by Rishi Raj et al., in 2010 [2], flash sintering has been attracting attention owing to its advantages over conventional sintering techniques [1,3]. Some advantages of flash sintering are high sintering efficiency at significantly lower furnace temperatures and higher sintering rates leading to shorter time durations. Due to these advantages, flash sintering has been widely employed for sintering numerous materials including ionic conductors [4–7], electronic ceramics [8], semiconductors [9,10], insulators [11–13], including some non-oxide ceramics and composites [14–16]. The flash sintering process is usually divided into three stages [17]; (a) A first incubation stage to prepare the start of the flash sintering process (Stage I). In this stage, the current and power are gradually increased with time, resulting in samples with no obvious shrinkage; (b) A second flash-sintering stage, in which the current and power are sharply increased within a few seconds leading to a simultaneous sample shrinkage (Stage II); (c) A third steady stage during which the supplied power is transformed from a constant voltage mode to a constant current mode (Stage III). In this stage, the samples are further densified and their microstructures altered.

In the experiments performed herein, densification mostly takes place during the flash sintering stage. However, the short duration of this stage(less than 5 s) makes it quite difficult to experimentally investigate the underlying rapid densification mechanism governing the flash sintering process. Thus, experimental studies on flash sintering carried out until now have mainly focused on flash events triggered during the incubation stage [18–20] and studying the effect of the electric field on the microstructure evolution during Stage III [10,21–23]. Undoubtedly, the potential mechanism governing the rapid densification process taking place during the flash-sintering stage is a hot topic. According to recent experimental and numerical investigations, joule heating may play a role in rapid densification [9,24], although flash sintering cannot be fully explained by this phenomenon [11,23,25,26]. Rishi Raj et al. proposed an alternative explanation based on the nucleation of Frenkel pairs [1,25]. While this theory explained the rapid increase of the sintering rate more satisfactorily, it failed to explain the incubation stage observed during flash sintering as suggested by Naik et al. [27]. In addition, the existence of Frenkel pairs is plausible although undemonstrated [28,29]. Thus, the underlying mechanism governing flash sintering and rapid densification still remains unknown.

In this paper, we investigated the densification kinetics during the flash sintering of a 3 mol% yttrium-stabilized zirconia (3YSZ) in the flashing stage (i.e. Stage II). Since the steady stage (Stage III) involves grain growth processes, it was ruled out by using a program-controlled power supply. Activation energy of the densification for the flash sintering process was obtained based on conventional sintering kinetics. It turned out that oxygen vacancies are dominant in controlling densification, and electrostatic interaction among polarized particles may account for the ultrafast densification.

2. Experimental procedure

A commercial high-purity 3YSZ powder (99.9% purity, Beijing

https://doi.org/10.1016/j.jallcom.2018.02.308
0925-8388/

HWRK Chem. Co., Beijing, China) was used as the raw material. Green bodies were consolidated from the 3YSZ powder into rectangular compacts by uniaxial pressing at 4MPa followed by cold isostatic pressing at 200MPa. The green bodies were subsequently pre-sintered at 900 °C for 4 h with the aim to burn out the blinder, obtain a theoretical green density of 49.5% and a cuboid of 18.7 mm × 3.52 mm × 1.44 mm.

A schematic diagram of the flash sintering test setup is shown in Fig. 1. The as-prepared sample was placed between two platinum plates, which also served as the electrodes for applying the DC electrical field. The shrinkage of sample was measured by a rebounding-type Linear Variable Differential Transformer (LVDT) apparatus, which was attached to the sample by an alumina pushrod. This LVDT apparatus could apply compression ranging from 15 g to 40 g through a built-in spring to alumina pushrod in order to accommodate the shrinkage. Accordingly, the sample was flash sintered under a maximum compression of 40 g (0.077 MPa), which was not enough to make difference in the flash sintering densification kinetics. In the case of flash sintering experiment, the furnace temperature was maintained at 900 °C for 30 min to reach a uniform temperature throughout the sample. First, an electric field of 95 V/cm was applied to the sample by a DC power supply (Sorenson DLM-300, Sorensen, San Diego, CA), and the preset current density limitation was set to 150 mA/mm^2. The power supply was immediately switched off by a programmed controller once the flash event occurred and the preset current limitation was attained. During this process, current and voltage readings were captured at 150 times per second. As indicated above, the flash sintering process studied herein lacked Stage III.

The kinetics of the flash sintering can be described based on the classical densification equation as follows [30]:

$$\frac{d\rho}{dt} = A\exp\left(\frac{-Q}{RT}\right)\frac{f(\rho)}{T * G^n} \quad (1)$$

where, $\frac{d\rho}{dt}$ is the densification rate; Q is the activation energy for the densification process; R is the gas constant; T is the absolute temperature; G is the grain size; n is a characteristic constant for a given densification mechanism (i.e. n = 3 and 4 correspond to lattice-diffusion and grain-boundary controlled densification processes, respectively); A is a material parameter that is insensitive to G, ρ or T; and $f(\rho)$ is a function of density that decreases or increases moderately as the density changes in a limited range within a frozen microstructure [31,32].

For isotropic shrinkage, the density during flash sintering (ρ) was given by the following equation [33]:

$$\rho = \frac{\rho_g}{\left(1 + \frac{\Delta l}{l_0}\right)^3} \quad (2)$$

where, ρ_g is the green density of sample, Δℓ is the dynamic linear shrinkage which can be measured with a precision of 10 μm in this work, and ℓ_0 is the original length of sample.

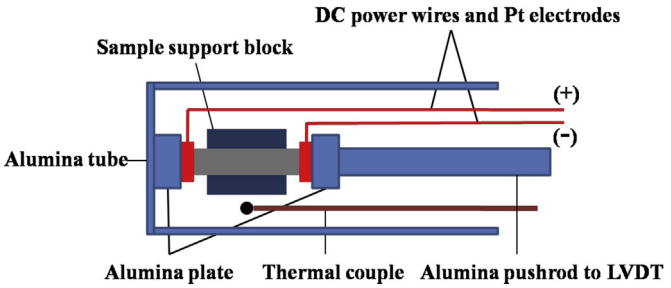

Fig. 1. Schematic of the apparatus used for flash sintering kinetics.

Combining Eqs. (1) and (2), the densification rate ($\frac{d\rho}{dt}$) in Eq. (1) is replaced by $\frac{d\Delta\ell}{dt}$, and Eq. (3) involving Δℓ is listed below:

$$\frac{d\Delta\ell}{dt} = B\exp\left(\frac{-Q}{RT}\right)\frac{g(\Delta\ell)}{T * G^n} \quad (3)$$

where, $\frac{d\Delta\ell}{dt}$ is the linear shrinkage rate, B is a material constant, and $g(\Delta\ell)$ is a function of linear shrinkage.

In the current analysis, it is assumed that $g(\Delta\ell)$ remains a constant when the linear shrinkage of samples changes in the range of 2% in a frozen microstructure. The densification process during flash sintering was divided into various periods with a 2% change interval in the linear shrinkage value. Given that G and $g(\Delta\ell)$ are held constant in the divided interval, we define a constant $C = B\frac{g(\Delta\ell)}{G^n}$, and take the natural logarithm on both sides of Eq. (3). The activation energy during flash sintering can then be measured through an Arrhenius formulation of $T * \frac{d\Delta\ell}{dt}$ and 1/T and expressed as:

$$\ln\left(T * \frac{d\Delta\ell}{dt}\right) = -\frac{Q}{RT} + \ln C \quad (4)$$

The density of the sintered bulk at the end of flash event was determined by the Archimedes method with distilled water as the immersion fluid. The microstructure and grain size of the sintered samples were characterized by field emission scanning electron microscopy (FESEM, S-4700, Hitachi, Tokyo, Japan).

3. Results and discussion

Greater current density led to larger linear shrinkage and higher relative density values, the relative density reached 90.6% via flash sintering without Stage III at a current density limit of 150mA/mm^2. Microstructures of the samples before and after flash sintering are shown in Fig. 2, with the average grain sizes measured as 161 ± 28 nm and 172.49 ± 31.14 nm, respectively. It should be noted that the average grain size remained nearly unchanged despite the increase in density with the current limits.

In a conventional sintering process, the sample is heated to elevated temperatures for certain time durations in order to obtain a higher density (i.e. a thermally activated process). During conventional sintering, the sample temperature can be accurately measured by a thermocouple. However, the direct measurement of the sample temperature during flash sintering is challenging. As a result, neither thermocouples nor conventional pyrometers are suited for this purpose because of their inadequate response times [9,26]. For this reason, the flash sintering temperature is usually estimated based on Joule heating using a black body radiation model [18,19,26,34]. Since the duration of the flash sintering stage (Stage II) is less than 5 s, we estimate the dynamic sample temperature according to the dynamic black body radiation model [26,34] as follows:

$$T_s = T_f + \int_0^t \frac{VI - A\sigma\varepsilon\left(T_s^4 - T_f^4\right)}{mc_p}dt \quad (5)$$

where, T_s is the sample temperature, T_f is the furnace temperature, VI is the input power dissipation, A is the surface area of the samples, σ is the Stefan's constant (5.67 x 10^{-8} W m^2/K^4), ε is the emissivity of the samples (0.9 in this study [34]), m is the mass of sample, and c_p is the heat capacity of 3YSZ, taken as 0.6 J g^{-1} K^{-1} [34]. Since the convection and conduction heat loss are omitted, the

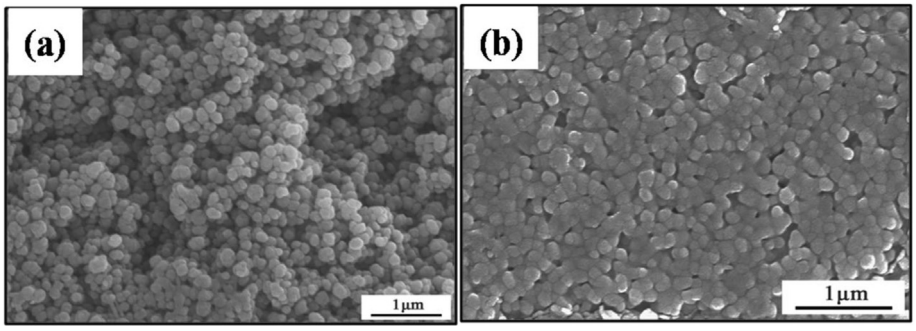

Fig. 2. Morphologies of the samples before and after flash event: (a) $j_{max} = 0$ mA/mm^2 and (b) $j_{max} = 150$ mA/mm^2.

sample temperature value may be slightly overestimated.

The dynamic linear shrinkage and estimated sample temperature during flash sintering according to Eq. (5) is plotted in Fig. 3. The start time of Stage II, t_{ini}, was defined as the time at the intersection point of the tangent lines corresponding to Stages I and II. In this study, the start of Stage II falls on the point where the current density is about 40 mA/mm^2. We used the estimated temperatures and the linear shrinkage rates of the flash sintering Stage I and II to fit Eq. (4). A series of parallel curves in the form of $\ln\left(T * \frac{d\rho}{dt}\right)$-1/T (Eq. (4)) were obtained, these curves resemble each other due to their similar y-intercepts (Fig. 4). As seen in Fig. 4, this curve can be fitted by two linear regression models with different slopes: one is a high gradient line corresponding to the incubation Stage I, and the other is a low gradient line corresponding to the flash-sintering Stage II. The values of densification activation energies, Q, can be calculated based on the slopes of the two linear fitting models. They are 313 ± 19 kJ/mol for Stage I, and 85 ± 7 kJ/mol for Stage II, respectively. Even though there are certain uncertainties in estimating the temperature, the obtained values were significantly different from the thermal activation energies of conventional sintered 3YSZ ceramics reported by Mazaheri et al. (485 ± 12 kJ/mol) [35] and Rishi Raj et al. (615 ± 80 kJ/mol) [36]. Clearly, the controlled flash sintering process of 3YSZ studied herein differed from a conventional densification process. Furthermore, different activation energies for Stage I and Stage II may suggest different densification mechanisms for these stages. As for the Stage I, the densification activation energy is about 313 kJ/mol lower than the conventional thermal activated densification

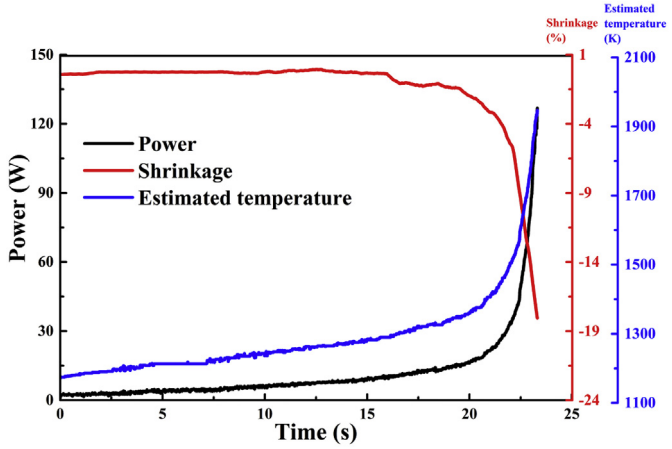

Fig. 3. Dynamic power dissipation, linear shrinkage and estimated sample temperature as a function of electric field application time.

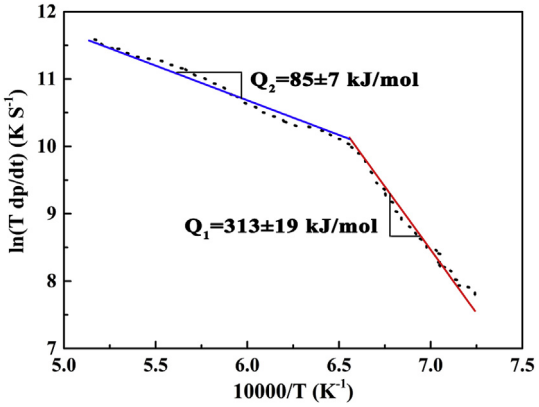

Fig. 4. Plot of $\ln\left(T \frac{d\rho}{dt}\right)$ as a function of reciprocal of the temperature of the flash-sintered samples.

process (Mazaheri et al. [35]). The applied threshold electrical field can not only disassociate the inherent associated $V_o^{\cdot\cdot}$ and Y'_{Zr} species but also inject extra oxygen vacancies into material [20]. The formation of abundant vacancies combined with the joule heating in Stage I might result in a lower densification activation energy compared to the pure thermally activated densification process.

Densification energies for Stage II show much lower value than that for the traditional thermal activated densification process, i.e. ~1/6 of the value reported by Mazaheri et al. [35]. It is noted that the activation energy for the conductivity of 3YSZ ceramics is ca. 105 kJ/mol [37,38], slightly higher than the activation energy for the densification process of Stage II studied herein. As reported by several authors [37–39], the conductivity of YSZ ceramics revealed two different contributions of the activation energy: (a) the disassociation energy of the associated oxygen vacancies ($V_o^{\cdot\cdot}$) and the doped ion (Y'_{Zr}) (ca. 25 kJ/mol theoretically), and (b) migration energy of oxygen vacancies (ca. 77 kJ/mol theoretically). The measured activation energy of the flash sintered 3YSZ sample was close to the migration energy of oxygen vacancies. Hence, we assumed that the migration of oxygen vacancies might be the process controlling densification during the flash sintering process of Stage II. The disassociation of associated $V_o^{\cdot\cdot}$ and Y'_{Zr} species and injection of extra oxygen vacancies occurred at the incubation stage (Stage I) under application of high voltage, as the previously reported [20]. The migration of oxygen vacancies appears to be the process controlling the densification.

However, the rapid shrinkage observed during the flash sintering stage cannot be fully explained by the migration of oxygen vacancies alone. Herein, we propose that Columbic force among particles contributes to the densification process based on our

experimental results. It is well known that defects having a net charge tend to form associated clusters due to Columbic forces. This phenomenon has been widely observed in numerous doped materials such as doped alumina [40] and zirconia [37]. When an electric field beyond a threshold value was applied to the 3YSZ samples, these associated clusters of $V_o^{\cdot\cdot}$ and Y'_{Zr} tend to separate and move along opposite directions of the electric field towards the particle surface [41] or the interface [25,42]. The number of accumulated charged defects ($V_o^{\cdot\cdot}$ and Y'_{Zr}) on the surface increases with time. When the number of charges on the surface is large enough, the adjacent particles are attracted to each other via Columbic forces, resulting in a charge avalanche and the ignition of the flash sintering process. Rapid shrinkage and quick densification not only occurred instantaneously but also simultaneously. The energy for the densification achieved via Columbic forces is very low and can be ignored for practical purposes. Thus, the activation energy for the densification process was either dominated by the charge accumulation process on the particle surface or the migration of oxygen vacancies to the particle surface. As a result, the extent of densification should depend on the Columbic force and the final relative density of the sintered 3YSZ samples should be determined by the number of charges on the particle or current density, in accordance with the experimental results. Since the densification via Columbic forces did not involve mass diffusion processes and the duration of the Stage II was limited, the particle size of the sintered 3YSZ samples should remain constant. It should be noted that specimen cannot reach fully dense via Columbic forces alone, the further densification including removal of pores and grain growth occurred at the steady stage (Stage III) of flash sintering.

4. Conclusion

The densification kinetics of flash sintered 3YSZ samples were investigated by controlling the maximum current density in the absence of steady stage (Stage III). 3YSZ showed an activation energy of 313 ± 19 kJ/mol for the incubation stage (Stage I), which is explained by the combination of Joule heating and the formation of oxygen vacancies under applied threshold electrical field. As for the flash sintering process (Stage II) the activation energy of ca. 85 ± 7 kJ/mol can be explained due to the migration of oxygen vacancies. These results indicate that the migration of oxygen vacancies could be the process controlling the flash sintering of 3YSZ once the flash sintering has been triggered. The Columbic force among polarized particles was proposed to contribute to the ultra rapid densification process during the Stage II flash sintering.

Acknowledgements

This work was financially supported by the National Natural Science Foundation of China (Grant# 51732009).

References

[1] R. Raj, M. Cologna, J.S. Francis, Methods of Flash Sintering: US, 2013. US 20130085055 A1[P].
[2] M. Cologna, B. Rashkova, R. Raj, Flash sintering of nanograin zirconia in <5 s at 850°C, J. Am. Ceram. Soc. 93 (2010) 3556–3559.
[3] S. Grasso, Y. Sakka, G. Maizza, Electric current activated/assisted sintering (ECAS): a review of patents 1906–2008, Sci. Technol. Adv. Mater. 10 (2009), 053001.
[4] J.M. Lebrun, T.G. Morrissey, J.S.C. Francis, et al., Emergence and extinction of a new phase during on–off experiments related to flash sintering of 3YSZ, J. Am. Ceram. Soc. 98 (2015) 1493–1497.
[5] O. Vasylkiv, H. Borodianska, Y. Sakka, et al., Flash spark plasma sintering of ultrafine yttria-stabilized zirconia ceramics, Scripta Mater. 121 (2016) 32–36.
[6] M. Cologna, A.L.G. Prette, R. Raj, Flash-sintering of cubic yttria-stabilized zirconia at 750°C for possible use in SOFC manufacturing, J. Am. Ceram. Soc. 94 (2011) 316–319.
[7] T. Jiang, Z. Wang, J. Zhang, et al., Understanding the flash sintering of rare-earth-doped ceria for solid oxide fuel cell, J. Am. Ceram. Soc. 98 (2015) 1717–1723.
[8] L.M. Jesus, R.S. Silva, R. Raj, et al., Electric field-assisted flash sintering of CaCu 3 Ti 4 O 12 : microstructure characteristics and dielectric properties, J. Alloy. Comp. 682 (2016) 753–758.
[9] Y. Zhang, J. Nie, J.M. Chan, et al., Probing the densification mechanisms during flash sintering of ZnO, Acta Mater. 125 (2017) 465–475.
[10] A. Karakuscu, M. Cologna, D. Yarotski, et al., Defect structure of flash-sintered strontium titanate, J. Am. Ceram. Soc. 95 (2012) 2531–2536.
[11] M. Cologna, J.S.C. Francis, R. Raj, Field assisted and flash sintering of alumina and its relationship to conductivity and MgO-doping, J. Eur. Ceram. Soc. 31 (2011) 2827–2837.
[12] I. Bajpai, Y.H. Han, J. Yun, et al., Preliminary investigation of hydroxyapatite microstructures prepared by flash sintering, Adv. Appl. Ceram 115 (2016) 276–281.
[13] L.A. Perez-Maqueda, E. Gil-Gonzalez, A. Perejon, et al., Flash sintering of highly insulating nanostructured phase-pure $BiFeO_3$, J. Am. Ceram. Soc. 100 (2017) 3365–3369.
[14] E. Bichaud, J.M. Chaix, C. Carry, et al., Flash sintering incubation in Al_2O_3/TZP composites, J. Eur. Ceram. Soc. 35 (2015) 2587–2592.
[15] D. Liu, Y. Gao, J. Liu, et al., SiC whisker reinforced ZrO_2 composites prepared by flash-sintering, J. Eur. Ceram. Soc. 36 (2016) 2051–2055.
[16] D. Demirskyi, O. Vasylkiv, Hot-spots generation, exaggerated grain growth and mechanical performance of silicon carbide bulks consolidated by flash spark plasma sintering, J. Alloy Compd. 691 (2017) 466–473.
[17] J.S.C. Francis, R. Raj, Influence of the field and the current limit on flash sintering at isothermal furnace temperatures, J. Am. Ceram. Soc. 96 (2013) 2754–2758.
[18] Y. Dong, I.W. Chen, Predicting the onset of flash sintering, J. Am. Ceram. Soc. 98 (2015) 2333–2335.
[19] R.I. Todd, E. Zapata-Solvas, R.S. Bonilla, et al., Electrical characteristics of flash sintering: thermal runaway of Joule heating, J. Eur. Ceram. Soc. 35 (2015) 1865–1877.
[20] Y. Gao, F. Liu, D. Liu, et al., Electrical-field induced nonlinear conductive behavior in dense zirconia ceramic, J. Mater. Sci. Technol. 33 (2017) 897–900.
[21] W. Qin, H. Majidi, J. Yun, et al., Electrode effects on microstructure formation during FLASH sintering of yttrium-stabilized zirconia, J. Am. Ceram. Soc. 99 (2016) 2253–2259.
[22] Y. Dong, H. Wang, I.W. Chen, Electrical and hydrogen reduction enhances kinetics in doped zirconia and ceria: I. Grain growth study, J. Am. Ceram. Soc. 100 (2016) 876–886.
[23] H. Yoshida, Y. Sakka, T. Yamamoto, et al., Densification behavior and microstructural development in undoped yttria prepared by flash-sintering, J. Eur. Ceram. Soc. 34 (2014) 991–1000.
[24] S. Grasso, E.Y. Kim, T. Saunders, et al., Ultra-rapid crystal growth of textured SiC using flash spark plasma sintering route, Cryst. Growth Des 16 (2016) 2317–2321.
[25] R. Raj, M. Cologna, J.S.C. Francis, Influence of externally imposed and internally generated electrical fields on grain growth, diffusional creep, sintering and related phenomena in ceramics, J. Am. Ceram. Soc. 94 (2011) 1941–1965.
[26] R. Raj, Joule heating during flash-sintering, J. Eur. Ceram. Soc. 32 (2012) 2293–2301.
[27] K.S. Naik, V.M. Sglavo, R. Raj, Flash sintering as a nucleation phenomenon and a model thereof, J. Eur. Ceram. Soc. 34 (2014) 4063–4067.
[28] K. Terauds, J.M. Lebrun, H.H, et al., Electroluminescence and the measurement of temperature during Stage III of flash sintering experiments, J. Eur. Ceram. Soc. 35 (2015) 3195–3199.
[29] J. Frenkel, On pre-breakdown phenomena in insulators and electronic semiconductors, Phys. Rev. 54 (1938) 647–648.
[30] J. Wang, R. Raj, Estimate of the activation energies for boundary diffusion from rate-controlled sintering of pure alumina, and alumina doped with zirconia or titania, J. Am. Ceram. Soc. 73 (1990) 1172–1175.
[31] James D. Hansen, et al., Combined-stage sintering model, J. Am. Ceram. Soc. 75 (1992) 1129–1135.
[32] I.W. Chen, X.H. Wang, Sintering dense nanocrystalline ceramics without final-stage grain growth, Nature 404 (2000) 168.
[33] D. Yang, R. Raj, H. Conrad, Enhanced sintering rate of zirconia (3Y-TZP) through the effect of a weak dc electric field on grain growth, J. Am. Ceram. Soc. 2010 (93) (2010) 2935–2937.
[34] W. Ji, B. Parker, S. Falco, et al., Ultra-fast firing: effect of heating rate on sintering of 3YSZ, with and without an electric field, J. Eur. Ceram. Soc. 37 (2017) 2547–2551.
[35] M. Mazaheri, A. Simchi, M. Dourandish, et al., Master sintering curves of a nanoscale 3Y-TZP powder compacts, Ceram. Int. 35 (2009) 547–554.
[36] J. Wang, R. Raj, Activation energy for the sintering of two-phase alumina/zirconia ceramics, J. Am. Ceram. Soc. 74 (1991) 1959–1963.
[37] W.C. Mackrodt, P.M. Woodrow, Theoretical estimates of point defect energies in cubic zirconia, J. Am. Ceram. Soc. 69 (1986) 277–280.
[38] D. Liu, Y. Cao, J. Liu, et al., Effect of oxygen partial pressure on temperature for onset of flash sintering 3YSZ, J. Eur. Ceram. Soc. 38 (2018) 817–820.
[39] V. Butler, C.R.A. Catlow, B.E.F. Fender, The defect structure of anion deficient

ZrO_2, Solid State Ionics 5 (1981) 539–542.
[40] K.P.D. Lagerlöf, R.W. Grimes, The defect chemistry of sapphire (α-Al_2O_3), Acta Mater. 46 (1998) 5689–5700.
[41] W.D. Kingery, Plausible concepts necessary and sufficient for interpretation of ceramic grain-boundary phenomena: I, grain-boundary characteristics, structure, and electrostatic potential, J. Am. Ceram. Soc. 57 (2010) 1–8.
[42] J.M. Lebrun, C.S. Hellberg, S.K. Jha, et al., In situ measurements of lattice expansion related to defect generation during flash sintering, J. Am. Ceram. Soc. 100 (2017) 4965–4970.

Ke Ren, Qiankun Wang, Yulong Lian, Yiguang Wang*

Science and Technology on Thermostructural Composite Materials Laboratory, Northwestern Polytechnical University, Xi'an, Shaanxi, 710072, PR China

* Corresponding author. Tel.: +86 2988494914.
E-mail address: wangyiguang@nwpu.edu.cn (Y. Wang).

5 January 2018
24 February 2018
26 February 2018
Available online 28 February 2018